AD-A155 019 A RANDOM LAYER MODEL FOR REFLECTION FROM OCEAN BOTTOM SEDIMENTS(U) SCIENCE APPLICATIONS INTERNATIONAL CORP MCLEAN VA R R GREENE ET AL. 08 FEB 85 SAIC-85/1036 1/1

UNCLASSIFIED N00014-83-C-0303 F/G 20/1 NL

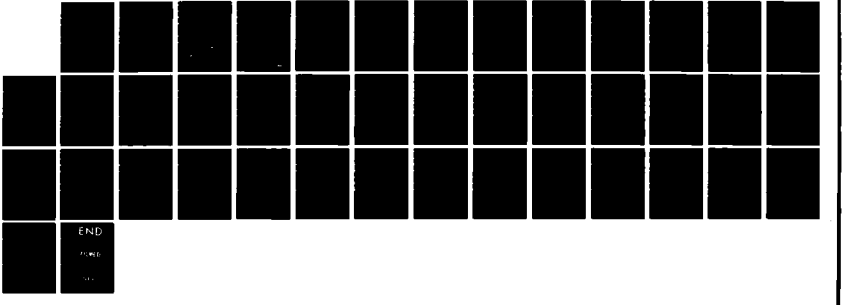

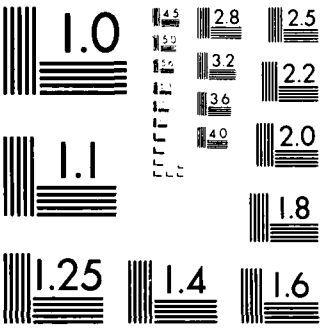

MICROCOPY RESOLUTION TEST CHART
NATIONAL BUREAU OF STANDARDS 1963-A

A RANDOM LAYER MODEL FOR REFLECTION FROM OCEAN BOTTOM SEDIMENTS

SAIC-85/1036

A RANDOM LAYER MODEL FOR REFLECTION FROM OCEAN BOTTOM SEDIMENTS

SAIC-85/1036

SAIC

Science Applications International Corporation

Post Office Box 1303, 1710 Goodridge Drive, McLean, Virginia 22102, (703) 821-4300

A RANDOM LAYER MODEL FOR REFLECTION FROM OCEAN BOTTOM SEDIMENTS

SAIC-85/1036

February 1985

Prepared
by

Robert R. Greene
David M. Rubenstein

Prepared
for

Naval Ocean Research
and Development Activity
NSTL Station, MS 39529

Contract No. N00014-83-C-0303

SCIENCE APPLICATIONS INTERNATIONAL CORPORATION

1710 Goodridge Drive
P.O. Box 1303
McLean, Virginia 22102
(703) 821-4300

SAIC
Science Applications
International Corporation

UNCLASSIFIED

SECURITY CLASSIFICATION OF THIS PAGE (When Data Entered)

REPORT DOCUMENTATION PAGE	READ DISTRUCTIONS BEFORE COMPLETING FORM
1. REPORT NUMBER: SAIC-85/1036	2. GOVT ACCESSION NO.: ADA150019
	3. RECIPIENT'S CATALOG NUMBER:
4. TITLE (and Subtitle): A Random Layer Model For Reflection From Ocean Bottom Sediments	5. TYPE OF REPORT & PERIOD COVERED: Technical Report
	6. PERFORMING ORG. REPORT NUMBER: SAIC-85/1036
7. AUTHOR(s): Robert R. Greene David Rubenstein	8. CONTRACT OR GRANT NUMBER(s): N00014-83-C-0303
9. PERFORMING ORGANIZATION NAME AND ADDRESS: Science Applications International Corp. 1710 Goodridge Drive, P.O. Box 1303 McLean, Virginia 22102	10. PROGRAM ELEMENT, PROJECT, TASK AREA & WORK UNIT NUMBERS: Task 3
11. CONTROLLING OFFICE NAME AND ADDRESS: Naval Ocean Research and Development Activity NSTL Station, MS 39529	12. REPORT DATE: Feb. 8, 1985
	13. NUMBER OF PAGES:
14. MONITORING AGENCY NAME & ADDRESS(if different from Controlling Office): Office of Naval Research Department of the Navy 800 N. Quincy Street Arlington, VA 22217	15. SECURITY CLASS. (of this report): Unclassified
	15a. DECLASSIFICATION/DOWNGRADING SCHEDULE:

16. DISTRIBUTION STATEMENT (of this Report)

Unlimited Distribution

17. DISTRIBUTION STATEMENT (of the abstract entered in Block 20, if different from Report)

18. SUPPLEMENTARY NOTES

19. KEY WORDS (Continue on reverse side if necessary and identify by block number)

Bottom Loss, Acoustic, Reflectivity, Sediment, Turbidites, Layering

20. ABSTRACT (Continue on reverse side if necessary and identify by block number)

Sub-bottom sediment layering is identified as the cause of strong acoustic reflectivity from the sea floor in abyssal plains. A technique for estimating the reflectivity from layering statistics in deep sea sediment cases is developed. Preliminary calculations are carried out which exhibit the qualitative and quantitative behavior of observed bottom reflectivity.

DD FORM 1473 EDITION OF 1 NOV 65 IS OBSOLETE
S/N 0102-LF-014-6601

UNCLASSIFIED

SECURITY CLASSIFICATION OF THIS PAGE (When Data Entered)

TABLE OF CONTENTS

LIST OF FIGURES

LIST OF TABLES

Section 1
INTRODUCTION

In this paper, a technique is developed which can be used to estimate the average reflectivity of ocean bottom sediments from the layering statistics of the sediment column. Gilbert[1] has addressed this problem with Monte Carlo simulation techniques. He published scatter diagrams of the distribution of the complex reflection coefficient from 30 realizations of a randomly layered sediment, showing the reflection coefficient becomes more random with higher frequency. Halthusen and Vidmar[2] published reflection loss curves for several realizations of randomly layered sediment. They show that reflection loss can be greatly reduced by the presence of layering. In this paper an analytical technique is developed for calculating the probability distribution of the complex reflection coefficient for a random ensemble of layered-structures. The average reflection loss calculated from this distribution is shown to agree quantitatively and qualitatively with observed data.

The reflectivity of the ocean bottom has been measured extensively on a worldwide basis by the Naval Air Defense Center and the Naval Oceanographic Office. A measurement is carried out by detonating SUS (Sound, Underwater Source) charges at various ranges from a stationary sonobuoy. The energy received in a given band (typically 1/3 or 1 octave between 50 and 1600 Hz) is integrated in time to obtain the total received intensity, I. The bottom loss (BL) is:

$$BL = -10 \log_{10}(I) + SL - TL,$$

where SL is the source level in dB, and TL is the transmission loss in dB along the path of propagation.

Near normal incidence each bottom-bounce arrival can be identified with a reflection from the sediment, no refracting paths being present. In practice, the reflection strengths are often quite strong, especially when the sediments are terrigenous in origin, as in the deep ocean abyssal plains. The observed bottom losses generally lie between 3 and 10 dB, corresponding to pressure reflection coefficients of magnitude .71 and .32 respectively. This is too strong to be accounted for by reflection from the water-sediment interface alone, which has a pressure reflection coefficient, due to density and sound speed discontinuities, of about .2, corresponding to a bottom loss of 14 dB. In this paper, it will be demonstrated that multiple reflection from many thin (~.25 - 1. m) sediment layers within the volume of the sediment can account for the strong reflectivity of terrigenous sediments.

Section 2

THE BOTTOM LOSS UPGRADE AND THE EXTRAPOLATION OF GEOACOUSTIC PARAMETERS

The Bottom Loss Upgrade[3,4,5] is a database of sediment thickness and eight parameters which characterize the acoustic properties of ocean bottom sediments. The data base is used to extend the sound velocity and attenuation profiles from the water column into the sediment, as shown in Figure 1. The sound speed profile depends on three parameters, which were chosen to be consistent with Hamilton's[6] canonical profiles for terrigenous, calcareous, and siliceous deep sea sediments. The attenuation profile is a linear function of depth. The two parameters of the attenuation profile are estimated from the strength of bottom refracted acoustic arrivals. Attenuation values agree with previously published data by Mitchell and Fock.[7] It was found that attenuation profiles were well correlated with physiographic province.

The last three parameters of the database characterize the reflectivity, or equivalently the input impedance, of the sediment, as described in Brekhovskikh.[8] It was found that the reflectivity of the bottom was generally stronger than would be expected from the density-sound-speed discontinuity at the water-sediment interface. The strongest reflectivity was observed in abyssal plains. Figures 2 and 3 are histograms of the minimum and maximum impedances of the sediment required to produce reflection strengths of the bottom observed in the NADC data. Figure 2 is compiled from data sets in terrigenous continental rise environments. Figure 3 is compiled from data sets in terrigenous abyssal plain environments. If the sediment is treated as a homogeneous fluid, its impedance would be the product of density

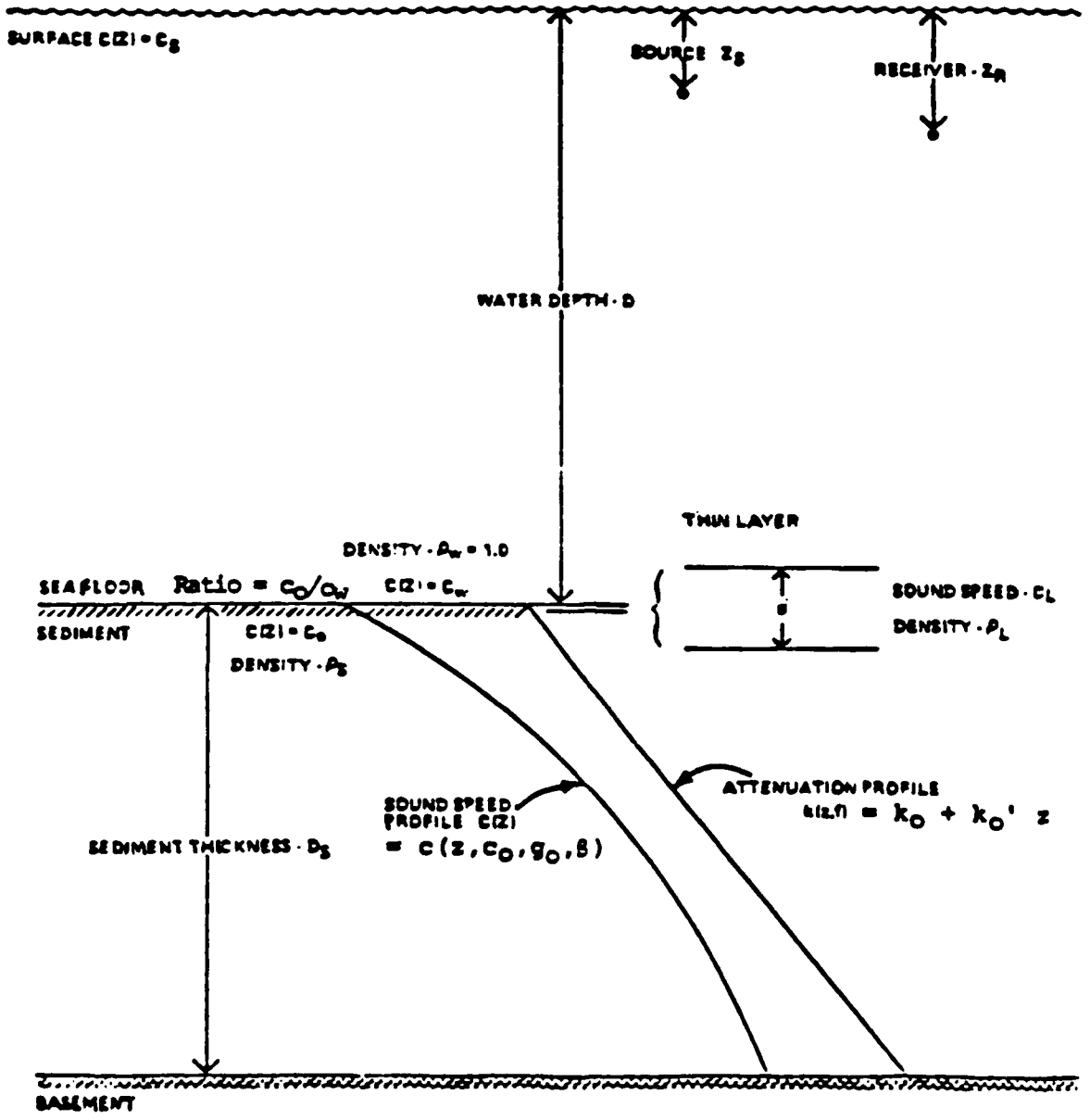

Figure 1. Geo-acoustic Parameters of the Bottom-Loss Upgrade Model

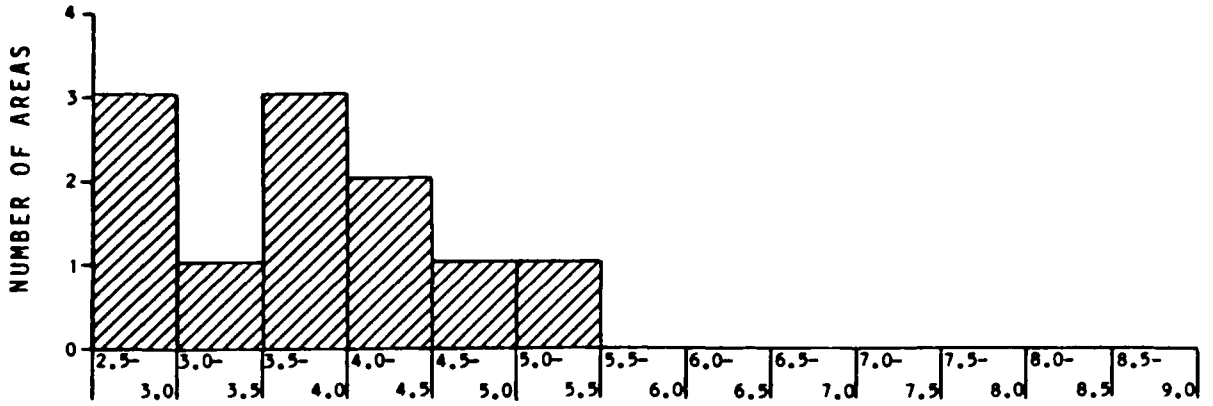

IMPEDANCE $Z_3 = \rho_3 \times 1.5$ km/s

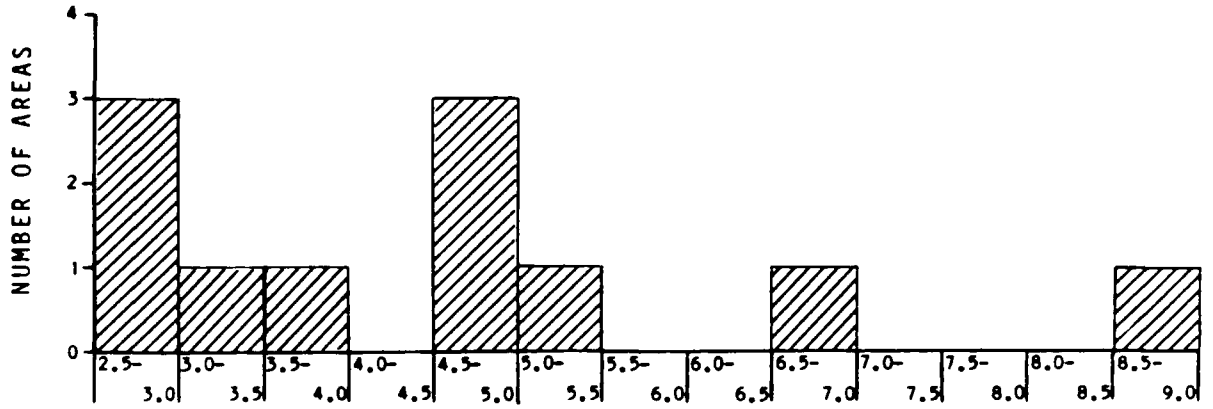

EFFECTIVE IMPEDANCE $Z_2' = \frac{Z_2^2}{Z_3} = \frac{(\rho_2 \times 1.5 \text{ km/s})^2}{(\rho_3 \times 1.5 \text{ km/s})}$

Figure 2. Effective Acoustic Impedance of the Ocean Bottom for Continental Rise Environments in the BLUG Database

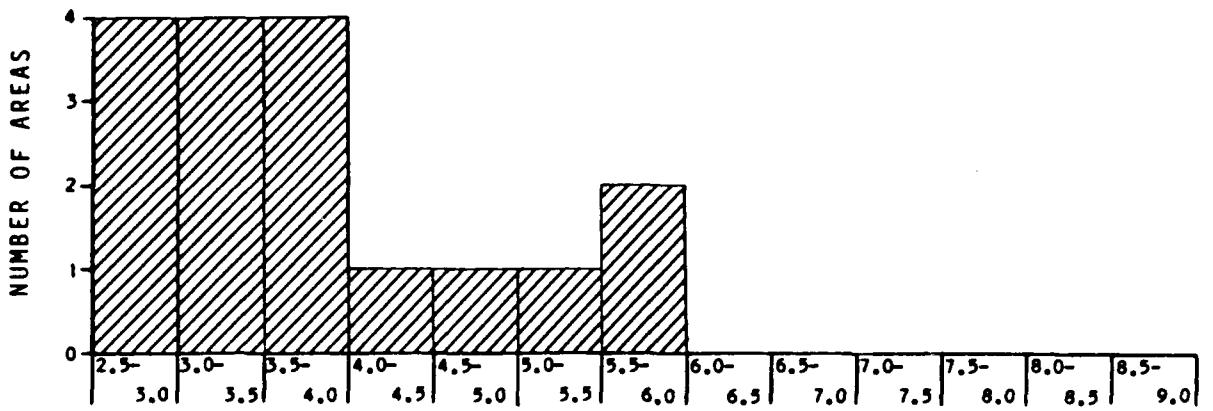

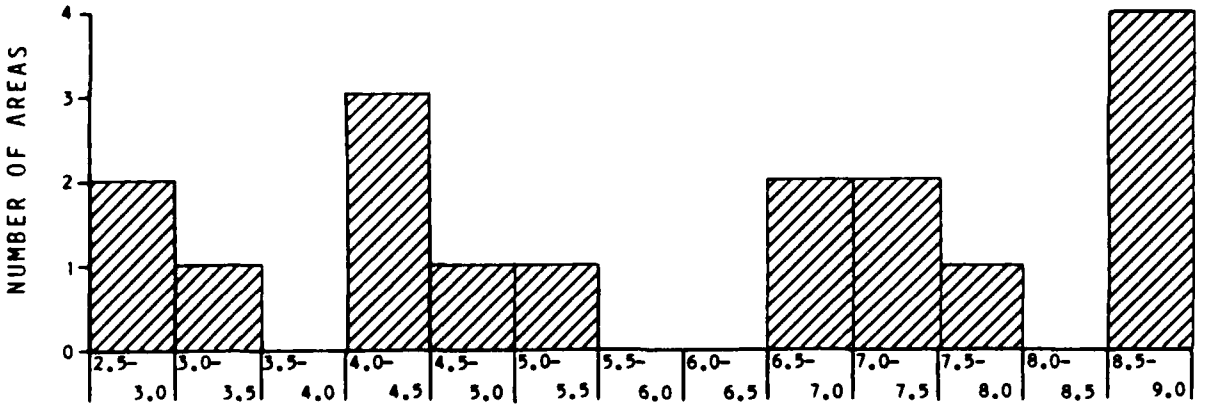

$$\text{EFFECTIVE IMPEDANCE } Z_2' = \frac{Z_2^2}{Z_3} = \frac{(\rho_2 \times 1.5 \text{ km/s})^2}{(\rho_3 \times 1.5 \text{ km/s})}$$

Figure 3. Effective Acoustic Impedance of the Ocean Bottom for Abyssal Plain Environments in the BLUG Database

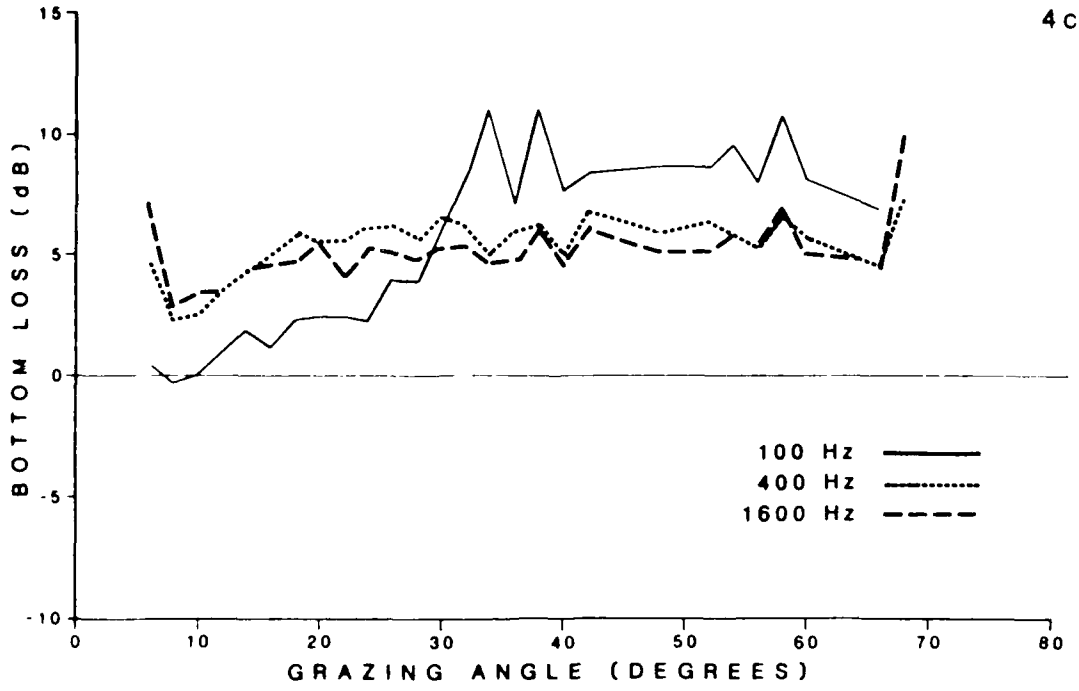
4c
BOTTOM LOSS (dB)
15
10
5
0
-5
-10
0
10
20
30
40
50
60
70
80
GRAZING ANGLE (DEGREES)
100 Hz
400 Hz
1600 Hz

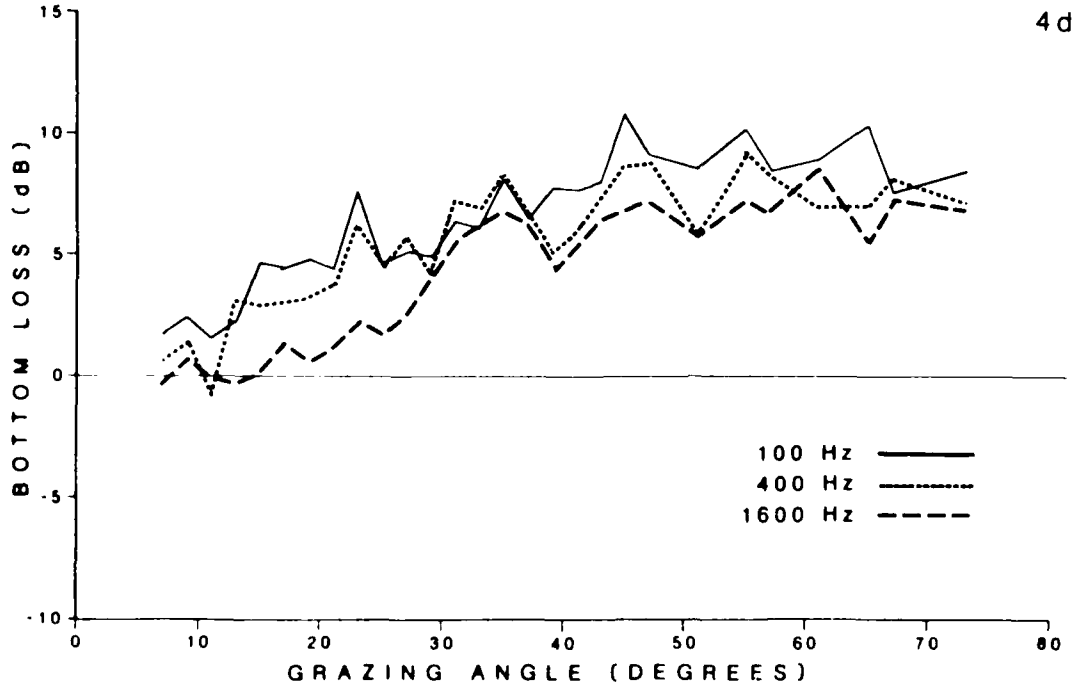
4d
BOTTOM LOSS (dB)
15
10
5
0
-5
-10
0
10
20
30
40
50
60
70
80
GRAZING ANGLE (DEGREES)
100 Hz
400 Hz
1600 Hz

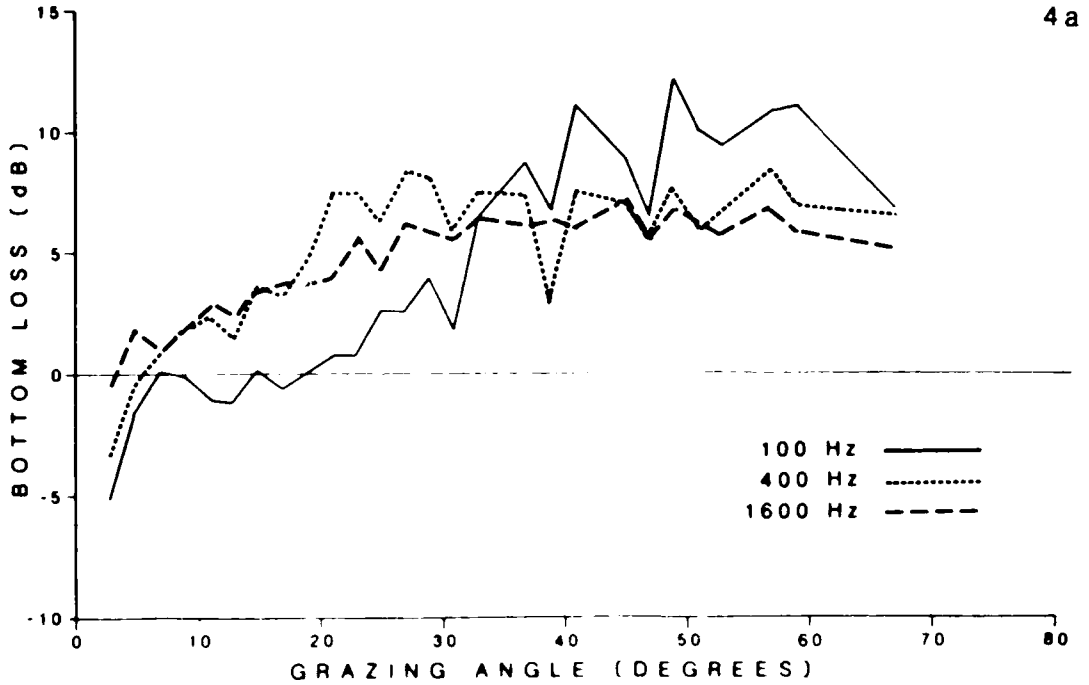

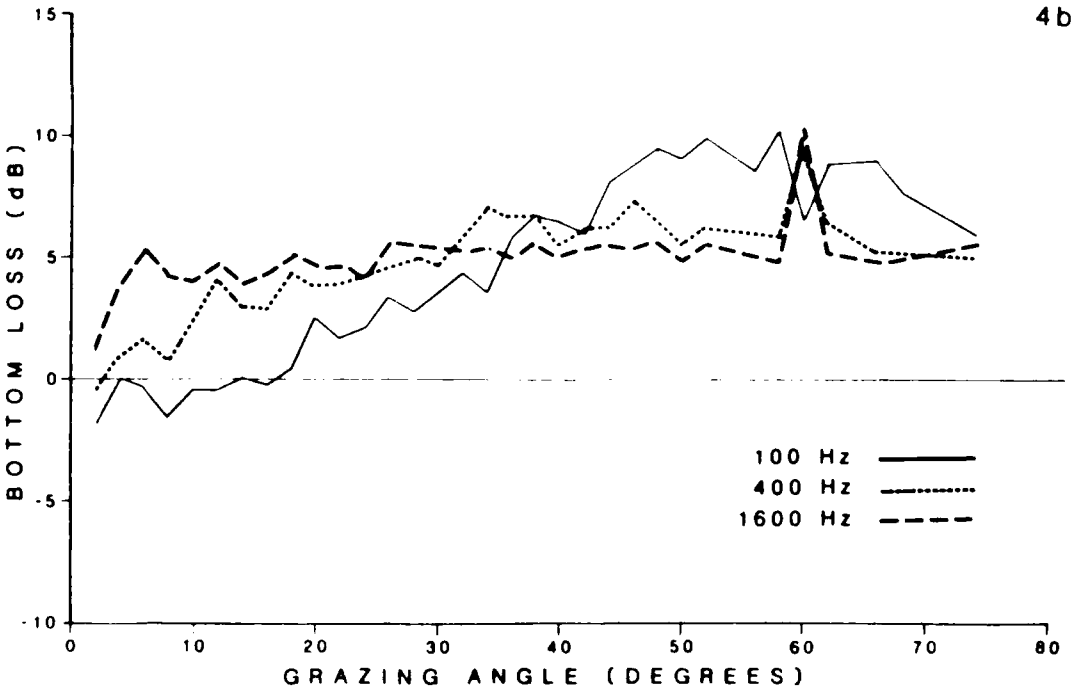

Figures 4a-4d. Measured Bottom Loss at Four Abyssal Plain Sites (pp. 3-12 and 3-13)

Section 5
MODEL-DATA COMPARISONS

5.1 PREDICTIONS AND COMPARISON WITH DATA

In abyssal plain environments, it is quite common for the reflection loss to be in the 5- to 10-dB range for large grazing angle. What is perhaps more surprising is that the reflection loss often decreases with frequency. This phenomenon is referred to as the negative frequency dependence of bottom loss. Figures 4-a through 4-d are examples of bottom loss which were measured in four abyssal plains at widely separated locations in the North Atlantic. Above about 35° grazing angle in these curves, the measured bottom loss becomes fairly level. In this range of angles the bottom interacting signal consists only of bottom reflecting paths, no refracting paths being present at short range. In each case, the reflection loss is much less than the 15-dB level attributed to reflection from the water-sediment interface. Furthermore, the loss at 1600 Hz is substantially less than the loss at 100 Hz. This is the negative frequency dependence phenomenon. The loss curve at 400 Hz is generally between the 100- and 1600-Hz curves, being closer to the 100-Hz curve at the lower angles and falling to the level of the 1600-Hz curve at the higher angles.

A prediction of average bottom loss values was carried out using the random periodic structure algorithm. The prediction was based on the geoacoustic model in Table 1:

For the purposes of the numerical implementation, a discrete sine transform was used for the u_j transform, giving an expression for the p_j in the form:

$$p_j(u_j,\theta_j)=\sum_{l=1}^{m}\left[\sum_{k=0}^{n} a_{kl}\sin(lu_j)\cos(k\theta_j)+\sum_{k=1}^{n} b_{kl}\sin(lu_j)\sin(k\theta_j)\right]. \tag{15}$$

The use of the sine transform guarantees the boundary condition $p_j(0,\theta_j) = 0$ on the boundary of the unit disk.

The 2nm+1 coefficients, a_{kl} and b_{kl}, in Eq. (15) are the $\tilde{p}_j$ in Eq. (9). The linear relationship between the coefficients of p_1 and p_2,

$$\tilde{p}_2 = A_1\,\tilde{p}_1 ,$$

is developed by evaluating Eq. (9) at 2nm+1 discrete values of $R_2 = e^{-i(u_2+i\theta_2)}$. This results in 2nm+1 independent linear equations relating the $\tilde{p}_2$ and $\tilde{p}_1$.

The mean value of intensity can be calculated from $p(u,\theta)$ using the formula:

$$\langle I\rangle = \int_0^{\infty}\int_0^{2\pi} p(u,\theta)\; e^{-4u}\; d\theta\, du\ . \tag{16}$$

periodic random structure using the formalism associated with Eq. (10).

A natural coordinate system was chosen for the implementation of Eq. (8). The following two substitutions are made, for the reflection coefficients R_2,

$$R_2 = e^{-(u_2+i\theta_2)} ,$$

and for $R_1 = L_t^{-1}(R_2)$,

$$L_t^{-1}(R_2) = e^{-2i\alpha t}\, e^{-(u_o+i\theta_o)},$$

where u_o and θ_o are chosen so that

$$e^{-(u_o+i\theta_o)} = \frac{R_2-r}{1-r^{*}R_2} .$$

Then Eq. (8) reduces to

$$p_2(u_2,\theta_2) = J_o^{-1}(R_2) \int_o^{\infty} p_1(u_o+\mathrm{Re}(\alpha)t, \theta_o+I_m(\alpha)t) \exp(4\cdot \mathrm{Im}(\alpha)t)\, \frac{e^{-t/D}}{D}\, dt . \qquad (13)$$

In this coordinate system, the probability densities can be expanded in a Fourier sine transform in u_j and a Fourier series in θ_j:

$$p_j(u_j,\theta_j) = \int_o^{\infty} \sin(\xi\, u_j)\Big[\sum_{k=0}^{n} a_k(\xi)\cos(k\theta_j) + \sum_{k=1}^{n} b_k \sin(k\theta_j)\Big]\, d\xi . \qquad (14)$$

as a Fourier Series, Eq. (8) can be used to construct a linear map from the expansion coefficients of p_1 to those of p_2:

$$\tilde{p}_2 = A_1 \tilde{p}_1 , \tag{10}$$

where A_1 is a matrix and $\tilde{p}_1$ and $\tilde{p}_2$ are the expansion coefficients of p_1 and p_2 respectively.

Similarly, if a second additional layer is added, a second relation:

$$\tilde{p}_3 = A_2 \tilde{p}_2 , \tag{11}$$

can be developed. In this paper, the special case of the periodic random structure is considered. When two types of layers, each with its own acoustical properties and thickness statistics, are alternated then the coefficients $\tilde{p}_1$ and $\tilde{p}_3$ must be identical. In this case, Eqs. (10) and (11) reduce to:

$$\tilde{p}_1 = A_2 A_1 \tilde{p}_1 . \tag{12}$$

Eq. (12) was implemented numerically by iteratively calculating the eigenfunction with eigenvalue closest to 1. When the process converged, the function p_1 corresponding to the expansion coefficients $\tilde{p}_1$ was found to be positive definite, as is required for a probability distribution.

An actual sequence of layers in ocean sediment is terminated at the top by the water-sediment interface. This final terminating layer can be added onto the top of the

choice of Ω. Thus for a given fixed layer thickness t, the following relation holds between p_1 and p_2:

$$p_2(R_2,t) = p_1\left(L_t^{-1}(R_2)\right) \exp\left(4 \cdot \mathrm{Im}(\alpha) t\right) J_0^{-1}(R_2) \ . \quad (7)$$

The random layered model is based on the probability distribution of the reflection coefficient when the layers have random thicknesses. This can be obtained by randomizing the density in Eq. (7) with respect to the thickness. The result is the expected value of p_2 with respect to the thickness:

$$\begin{aligned} p_2(R_2) &= \int_0^\infty p_2(R_2,t) \frac{e^{-t/D}}{D} \, dt \\ &= J_0^{-1}(R_2) \int_0^\infty p_1\left(L_t^{-1}(R_2)\right) \exp\left(4 \cdot \mathrm{Im}(\alpha) t\right) \frac{e^{-t/D}}{D} \, dt, \end{aligned} \quad (8)$$

where the expression $L_t^{-1}(R_2)$ is

$$L_t^{-1}(R_2) = e^{-2i\alpha t} \frac{R_2 - r}{1 - r^* R_2} \ , \quad (9)$$

and D is the mean layer thickness. The probability density of a sequence of layers of random thickness can be calculated recursively using Eq. (8), by adding layers to the top of the sequence one by one.

4.2 NUMERICAL IMPLEMENTATION

When the probability densities p_1 and p_2 are expanded in terms of a set of basis functions, for instance

for complex reflection coefficient r, where r^* is the complex conjugate of r. Eq. (2) has the advantage of maintaining conservation of energy and reduces to Eq. (1) for real values of r.

When an additional layer of specified thickness t is added to the top of the sediment sequence, the probability densities for R_1 and R_2, $p_1(R_1)$ and $p_2(R_2,t)$ respectively, are defined in the complex unit disk, and satisfy the following identity:

$$\int_{\Omega} p_2(R_2,t)\, dx_2\, dy_2 = \int_{L_t^{-1}(\Omega)} p_1(R_1)\, dx_1\, dy_1 , \quad (3)$$

where Ω is any sufficiently well-behaved region in the unit disk. From Eq. (3) it is possible to derive an algebraic relationship between $p_1(R_1)$ and $p_2(R_2,t)$. By simply changing variables in the second integral, there results:

$$\int_{\Omega} p_2(R_2,t)\, dx_2\, dy_2 = \int_{\Omega} p_1\left(L_t^{-1}(R_2)\right) J_t^{-1}(R_2)\, dx_2\, dy_2 . \quad (4)$$

Here, J_t^{-1} is simply the Jacobian of $L_t^{-1}(R_2)$ which is:

$$J_t^{-1} = \exp\left(4 \cdot \mathrm{Im}(\alpha)\ t\right) \frac{\left(1-|r|^2\right)^2}{1-r^*|R_2|^4} \quad (5)$$

$$= \exp\left(4 \cdot \mathrm{Im}(\alpha)\ t\right) J_0^{-1}(R_2) . \quad (6)$$

It is a simple consequence of analysis that the integrands of Eq. (4) must be equal, since Eq. (4) holds for an arbitrary

coefficient of the new sequence can be calculated from that of the previous sequence according to the formula:

$$R_2 = \frac{r + R_1 e^{2i\alpha t}}{1 + rR_1 e^{2i\alpha t}} = L_t(R_1) \ , \qquad (1)$$

where

R_1 is the reflection coefficient of the original layer sequence,

R_2 is the reflection coefficient of the sequence with the addition of one new layer,

r is the reflection coefficient of the interface at the top of the new layer,

t is the thickness of the layer, and

α is $k \sin\theta$, the wavenumber times the sign of the grazing angle.

Attenuation is formally added to acoustic propagation through the use of complex sound speeds. In this case, the grazing angle θ, the vertical wave number α, and the reflection coefficient r become complex. For a real reflection coefficient r, Eq. (1) maintains conservation of energy, that is, when $|R_1| \leq 1$ then $|R_2| \leq 1$. However, when r becomes complex, Eq. (1) no longer conserves energy, and can produce reflection coefficients greater than one. For the purposes of this paper, Eq. (1) will be generalized to:

$$R_2 = L(R_1) = \frac{r + R_1 e^{2i\alpha t}}{1 + r^* R_1 e^{2i\alpha t}} \ , \qquad (2)$$

Section 4
DISTRIBUTION OF THE REFLECTION COEFFICIENT

4.1 MATHEMATICAL FORMULATION

In this section, the probability distribution for the reflection coefficient from a sequence of layers of random thickness is developed. This is done by adding layers one by one onto the top of the sequence. At each step of this process, the distribution of the reflection coefficient R_n for the n-layer system is calculated from the distribution of the reflection coefficient R_{n-1} of the n-1 layer system. In this way, the acoustic properties of fairly complex layered sequences can be developed.

In this paper, the case of the periodic random structure is analyzed. In this case the sediment consists of two materials (i.e., mud and sand) which proceed to infinite depth in alternating layers of random thickness. The probability distribution of interest is the distribution of the reflection coefficient over the entire ensemble of possible layer thicknesses. The advantage of the periodic random structure is that if one additional pair of mud and sand layers, each with random thickness, is added to the structure, then the ensemble of possible random layered structures constructed is identical to the original ensemble. Thus the statistical properties of the layered system are periodic, even though some individual realization of the layered structure is not.

When an additional reflecting layer is added to the top of a sequence of reflecting layers, the reflection

the slump. The thickness of the large grain layers is probably proportional to the amount of sediment on the continental shelf available for transport, which also increases proportionally with time.

In the model of sediment thickness used here, the waiting time between slump events is assumed to be a random variable with exponential distribution. Accordingly, the thicknesses of the large grain and small grain layers are assumed to be exponentially distributed random variables. For simplicity it is assumed that the thickness of each layer is independent of the thickness of the other layers. The exponential distribution function has the explicit form:

$$F(d) = 1 - \exp(-d/D),$$

with the associated density:

$$f(d) = \frac{1}{D} \exp(-d/D),$$

where d is the random variable of layer thickness and D is the mean layer thickness. The large grain and small grain layers are assigned different mean thickness values, the small grain layers generally being the thicker. The exponential distribution is often referred to as the waiting time distribution. This is because if some number of events occur at random times within a given time interval, the waiting time between the individual events will be distributed according to the exponential distribution.

For the purposes of calculation, the geo-acoustic properties, such as sound speed, density, and attenuation, will be assigned fixed values appropriate to the type of sediment. While the actual sound speed and density may vary from, say, sand layer to sand layer, the variation is small. This can be seen in measurements published by Hamilton,[17] Horn,[18] and Tucholke.[19]

enough, the sediment can be transported to great distances. By 1965, Potter and Schiedegger[16] demonstrated a good correlation between the thickness of the graded bed and the grain size in turbidite sediments. They showed that the empirical relation between grain size and bed thickness is consistent with predictions of the rate of sediment deposition based on the decay of turbulence in a turbidity current.

3.2 THE GEOPHYSICAL MODEL

At frequencies below 1600 Hz sound can penetrate the sea floor sediment for tens or even hundreds of meters and be reflected back into the water column. Information on sediment layering from sediment cores is generally only available for at most about 10 meters. Properties of sediment layering below the core can at best be characterized statistically. In this section a simple statistical model of sediment layering will be developed based on the sedimentation process.

The sediment column in abyssal plains is composed of alternating layers of large and small grain material. The large grain material is laid down by discrete short-term events associated with the slump of sediment off the continental shelf and transported by turbidity currents. Between the slumping events, smaller grain material is laid down continuously by the more gradual processes of sedimentation in the deep sea.

In both types of sedimentation process, it is reasonable to assume that the thickness of the layers is proportional to the time between the slumping events. The finer grain layers build up continuously until interrupted by

Section 3
SEDIMENT STRUCTURE

3.1 NEAR SURFACE SEDIMENT LAYERING

Near surface sediment layering in abyssal plain sediments has been observed for many years using high resolution echo sounders. Sub-bottom reflections were first observed in a series of cruises by the Woods Hole Oceanographic Institution between 1958 and 1962, and reported by Hersey and Rutstein,[9] Worzel,[10] Heezen, et al.,[11] and Menard.[12] In 1959, Worzel[10] identified a particular sub-bottom reflection in the southeastern Pacific with an ash layer observed in sediment cores.

In 1965, Hersey[13] published echo sounding from several locations in the North Atlantic Ocean and Mediterranean Sea. He identified observed sub-bottom reflectors with alternating layers of sorted coarse clastic materials and clays. The clastic materials were either sorted sand and silt, laid down by sediment turbidity currents, or volcanic ash.

According to Sadler,[14] turbidity currents were first proposed as a mechanism for the deposition of graded sediment beds by Kuenen and Migliorini[15] in 1950. A turbidity current is a suspension of sediment in seawater which flows down the continental slope and spreads out on the ocean floor. Settling of the suspended sediment load is retarded by turbulence as the current moves down the slope. Gradually, the load drops out in an abyssal plain as the current slackens. If the initial velocity of the sediment is high

(~1.5 g/cc) and sound speed (~1.5 km/sec), approximately 2.25. As can be seen in Figures 2 and 3, the required impedance is always greater than 2.25, and tends to be somewhat higher in abyssal plain environments than in the continental rise environments.

During the development of the Bottom Loss Upgrade, it was necessary to extrapolate the acoustic properties of a given region of the ocean bottom to other regions where no data was available. It was readily apparent from the acoustic data that abyssal plains exhibit strong reflectivity. However, the actual level of reflectivity did not seem to be related to the average geophysical properties of the sediment column. It was decided to extrapolate the geoacoustic parameters from area to area based on the observed or surmised presence of layering in the sediment. As a primary goal, it was desirable to verify that this was a viable technique. The optimum solution to the problem would be a direct method of estimating acoustic reflectivity from the observed layering in available core data. This paper presents preliminary results in this direction.

Table 1

TRIAL GEOACOUSTIC MODEL FOR BOTTOM LOSS PREDICTIONS

MATERIAL	DENSITY RATIO re/Water	SOUND SPEED RATIO re/Water	MEAN LAYER THICKNESS	ATTENUATION dB/m/kHz
Water	1	1	N/A	0
Silty Clay	1.5	.996	1.0 Meter	.015
Sand-Silt-Clay	1.7	1.004	.25 Meter	.015

The density values were increased slightly from near-surface values to approximate those at a few tens-of-meters depth, although bottom loss estimates depend only on the ratio of the two values.

The following values (in Table 2) of mean reflected intensity, expressed in dB, were calculated based on the values in Table 1:

Table 2

ESTIMATED BOTTOM LOSS IN dB BASED ON THE GEOACOUSTIC MODEL IN TABLE 1

40° Grazing	
Freq Hz	<Loss> dB
100	7.49
400	7.68
1600	5.29

80° Grazing	
Freq Hz	<Loss> dB
100	7.58
400	4.96
1600	4.64

The calculated loss levels are in good agreement with the four cases of measured loss in Figures 4-a through 4-d. At both the 40° grazing and 80° grazing angles, the loss at 1600 Hz lies below the loss at 100 Hz. The 400-Hz value lies above the 1600-Hz value at the 40° grazing angle and moves down to the 1600-Hz value at the 80° grazing angle. For this simple case, the model for scattering from sub-bottom reflectors in the form of sediment layers of random thickness seems to account for both the observed levels and the negative frequency dependence of observed bottom loss using realistic values of geoacoustic sediment properties and layering statistics.

5.2 LIMITATIONS

The algorithm for calculating the mean value of loss based on Eq. (8) has the disadvantage that a large number of terms in the two-dimensional series expansion of the probability density must be calculated. The calculation of the N coefficients then depends on iteration using an NxN matrix. The large memory requirements of this algorithm may limit the number of terms carried. The algorithm has yet to be extensively tested. In particular, the sensitivity of the results to the number of coefficients is unknown.

Section 6
CONCLUSIONS

A procedure for estimating reflection losses from layered ocean bottom sediments, such as those observed in abyssal plains, has been implemented. Limited experience with it indicates that it can reproduce observed reflection loss levels using the geoacoustic properties and layering statistics of ocean bottom sediments. Furthermore, it reproduces the observed qualitative dependence of reflection loss on angle and frequency, including the negative frequency dependence.

Section 7
ACKNOWLEDGMENTS

This work was funded by the Bottom Interaction Program under Contract No. N00014-83-C-0303. Special thanks are given to William F. Monet, Dr. Richard Bachman, and Dr. Brackett Hersey for supplying references and advice on the geology of ocean bottom sediments.

Section 8
REFERENCES

1. K. E. Gilbert, "Reflection of Sound from a Randomly Layered Ocean Bottom," J. Acoust. Soc. Am. 68(5), 1454-1458 (1980.

2. H. Holthusen and P. A. Vidmar, "The Effect of Near-Surface Layering on the Reflectivity of the Ocean Bottom," J. Acoust. Soc. Am. 72(1), 226-234 (1982).

3. C. W. Spofford, R. R. Greene, and J. B. Hersey, "The Estimation of Geo-acoustic Ocean-sediment Parameters from Measured Bottom-loss Data," SAIC Report SAI-83-879-WA, March 1983.

4. W. F. Monet, R. R. Greene, and C. W. Spofford, "Development of Geo-Acoustic Areas for the Bottom Loss Upgrade," SAIC Report SAI-83-976-WA, March 1983.

5. R. R. Greene and C. W. Spofford, "Comparisons of NADC Measured Bottom Loss with BLUG Simulated Bottom Loss," SAIC Report SAI-84-138-WA, March 1983.

6. E. L. Hamilton, "Sound Velocity Gradients in Marine Sediments," J. Acoust. Soc. Am. 65(4), 909-922 (1979).

7. S. K. Mitchell and K. C. Focke, "New Measurements of Compressional Wave Attenuation in Deep Ocean Sediments," J. Acoust. Soc. Am. 67(5), 1582-1589 (1980).

8. L. M. Brekhovskikh, Waves in Layered Media, (Academic Press, New York, 1960), pp. 56-61.

9. J. B. Hersey and M. S. Rutstein, "Reconnaissance Survey of Oriente Deep (Caribbean Sea) With a Precision Echo Sounder," Geol. Soc. America Bull. 69, 1297-1304 (1958).

10. J. L. Worzel, "Extensive Deep Sea Sub-bottom Reflections Identified as White Ash," Natl. Acad. Sci. Proc. 45, 349-355 (1959).

11. B. C. Heezen, M. Thorpe, and M. Ewing, "The Floors of the Oceans: I. The North Atlantic," Geol. Soc. Am. Special Paper 65 (1959).

12. H. W. Menard, Marine Geology of the Pacific (McGraw Hill Book Co., New York, 1964).

13. J. B. Hersey, "Sediment Ponding in the Deep Sea," Geol. Soc. Am. Bull. 76, 1251-1260 (1965).

14. P. M. Sadler, "Bed-thickness and Grain Size of Turbidites," Sedimentology 29, 37-51 (1982).

15. P. H. Kuenen and C. I. Migliorini, "Turbidity Currents as a Cause of Graded Bedding," J. Geol. 58, 91-127 (1950).

16. P. E. Potter and A. E. Scheidegger, "Bed Thickness and Grain Size: Graded Beds," Sedimentology 1, 233-240 (1966).

17. E. L. Hamilton, "Geoacoustic Modeling of the Sea Floor," J. Acoust. Soc. Am. 68, 1313-1340 (1980).

18. D. R. Horn, M. Ewing, B. M. Horn, and M. N. Delach, "A Prediction of Sonic Properties of Deep-Sea Cores, Hatteras Abyssal Plain and Environs," Lamont-Doherty Geological Observatory Technical Report No. 1, November 1969.

19. B. E. Tucholke, "Acoustic Environment of the Hatteras and Nares Abyssal Plains, Western North Atlantic Ocean, Determined from Velocities and Physical Properties of Sediment Cores," J. Acoust. Soc. Am. 68, 1376-1390 (1980).

Section 9

SUPPLEMENTAL DISTRIBUTION LIST

Bachman, Dick
Naval Ocean Systems Center
Building 305
San Diego, CA 92152

Baer, Ralph N.
Naval Research Laboratory
Code 5160
Large Aperture Acoustics Branch
Washington, D.C. 20375

Baggeroer, Dr. Arthur
Department of Ocean Engineering
Massachusetts Inst. of Technology
Cambridge, MA 02139

Besieris, Dr. I.M.
Virginia Polytechnic Inst. &
State University
Dept. of Electrical Engineering
Blacksburg, VA 24061

Brown, Dr. Michael
Rosentier School of Marine &
Atmospheric Science
4600 Rickenbacker Causeway
Miami, FL 33149

Brunson, Burlie A.
Planning Systems, Inc.
7900 West Park Drive
Suite 600
McLean, VA 22102

Buck, Beumont M.
Polar Research Laboratory
123 Santa Barbara St.
Santa Barbara, CA 93101

Bucker, Dr. Homer
Naval Ocean Systems Center
Code 5311
San Diego, CA 92152

Burridge, Prof. Robert
Courant Inst. of Mathematical Sciences
New York University
251 Mercer Street
New York, NY 10012

Cable, Dr. Peter
Naval Underwater Systems Center
New London, CT 06230

Cavanaugh, Dr. Ray
Planning Systems, Inc.
7900 Westpark Drive
McLean, VA 22102

Chin-Bing, Stan
NORDA
NSTL Station, MS 39529

Clay, Prof. Clarence S.
University of Wisconsin
Dept. of Geology & Geophysics
Weeks Hall for Geological Sciences
Madison, WI 53706

Dantzler, CDR L.
U.S. Naval Observatory
OP 952
34th & Massachusetts Ave., N.W.
Washington, DC 20390

Dashen, Prof. Roger
The School of Natural Sciences
The Inst. of Advanced Study
Princeton, NJ 08540

Deavenport, Dr. Roy
Naval Underwater Systems Center
New London, CT 06230

DeFerrari, Dr. Harry A.
University of Miami
Rosentiel School of Marine and
Atmospheric Science
Miami, FL 33149

Diachok, Dr. Orest
Naval Research Laboratory
Code 8168
Washington, DC 20375

Dicus, Ronald L.
Naval Research Laboratory
Code 5160
Washington, D.C. 20375

DiNapoli, Dr. Fred
Naval Underwater Systems Center
New London, CT 06230

Dyer, Dr. Ira
Massachusetts Inst. of Technology
Department of Ocean Engineering
Cambridge, MA 02139

Eller, Anthony I.
NORDA Laison Office
800 North Quincy Street
Room 522
Arlington, VA 22217-5000

Farwell, Robert W.
Code 115
NORDA
NSTL, MS 39529-5004

Fauquet, LCDR R.
U.S. Naval Observatory
OP 952
34th & Massachusetts Ave., N.W.
Washington, DC 20390

Felsen, Dr. L. B.
Polytechnic Inst. of New York
Dept. of Electrical Engineering
Route 110
Farmingdale, NY 11735

Francois, Dr. R. E.
University of Washington
Applied Physics Laboratory
1013 N.E. 40th Street
Seattle, WA 98105

Hamilton, Edwin L.
Naval Ocean Systems Center
Code 5311 (T) Building 305
San Diego, CA 92152

Harlett, CAPT John
Office of Naval Technology
800 N. Quincy St.
Arlington, VA 22217

Harper, Dr. Edward J.
Office of the Chief of Naval Operations
OP-21T
The Pentagon, Rm 4D 544
Washington, DC 20350

Hawker, Dr. Ken
PME 124
6N08 NC1
Naval Electronics Systems Command
Washington, DC 20360

Henrick, Dr. Robert F.
Applied Physics Laboratory
Building 7, Room 326
Johns Hopkins University
Johns Hopkins Rd.
Laurel, MD 20707

Hibler, Dr. W. D., III
Snow and Ice Branch
U.S. Army Cold Regions Research &
Engineering Laboratory
Hanover, NH 03755

Holford, Dr. Richard
Bell Laboratories
Room 4C-240-B
Whippany Road
Whippany, NJ 07834

Hollis, CDR Steven
NAVELEX 612
Washington, DC 20360

Houser, Dale
NAVSEA 63R1
Washington, DC 20362

Jackson, Daryl
University of Washington
Applied Physics Laboratory
1013 N.E. 40th Street
Seattle, WA 98105

Jacobson, Melvin J.
Rensselaer Polytechnic Institute
Department of Mathematical Sciences
Troy, NY 12181

Jobst, Bill
NAVOCEANO
NSTL Station, MS 39529

Keenan, Ruth
1 Piccadilly Road
Sandwich, MA 02563

Kinney, Wayne
NORDA
NSTL Station, MS 39529

Kohler, Dr. Werner E.
Dept. of Mathematics
VA Polytechnic Inst. and
State University
Blacksburg, VA 24061

Kuperman, Dr. William
Numerical Modelling Division
Naval Ocean Research & Development Activity
Code 320
NSTL Station
Bay St. Louis, MS 39529

Kutschale, Dr. H. W.
Columbia University
Lamont-Doherty Geological Observatory
Palisades, NY 10964

Labianca, Dr. Frank M.
Signal Processing Research Dept.
Bell Laboratories
Whippany Road
Whippany, NJ 07891

Lee, Dr. Ding
Naval Underwater Systems Center
New London Laboratory
New London, CT 06320

Lyons, Dr. Waldo
Naval Ocean Systems Center
Arctic Submarine Laboratory
San Diego, CA 92152

Martin, Dr. Bob
Naval Ocean Research & Development Activity
NSTL Station
Bay St. Louis, MS 39529

McCammon, Diana F.
Pennsylvania State University
Applied Rersearch Laboratory
State College, PA 16801

McCoy, Dr. John
Dept. of Civil Engineering
The Catholic University of America
Washington, DC 20064

McDaniel, Dr. Suzanne T.
Pennsylvania State University
Applied Research Laboratory
State College, PA 16801

Mikhalevsky, Dr. Peter N.
OP 95T
Washington, DC 20310

Morrison, Dr. James
University of Washington
Applied Physics Laboratory/
Polar Science Center
Seattle, WA 98195

Moseley, Dr. William
Naval Ocean Research & Development Activity
NSTL Station
Bay St. Louis, MS 39529

Munk, Dr. Walter
Scripps Inst. of Oceanography
Inst. of Geography & Planetary Physics
University of California, San Diego
San Diego, CA 92093

Novick, Arnie
Mission Sciences Corp.
6090 Jericho Turnpike
Kommack, NY 11725

Paquin, James
Planning Systems, Inc.
1508 Gause Boulevard, Suite 204
Slidell, LA 70458

Pierce, Allan D.
Georgia Institute of Technology
School of Mechanical Engineering
Atlanta, GA 30332

Porter, Dan
NAVSEA 63R1
Washington, DC 20362

Posey, Joe
NORDA
NSTL Station, MS 39529

Pritchard, Dr. R. S.
Flow Research Company
Kent, WA 98301

Ramsdale, D.
NAVAIR 370
Washington, DC 20361

Roderick, Dr. William
Naval Underwater Systems Center
New London, CT 06320

Rogers, Peter H.
7709 Ivymount Terrace
Potomac, MD 20854

Root, Richard
NORDA
Code 115
NSTL, MS 39529-5004

Sabol, CAPT E. J.
Naval Ocean Systems Center
Arctic Submarine Laboratory
San Diego, CA 92152

Schulkin, Dr. Morris
University of Washington
Applied Physics Laboratory
Seattle, WA 98105

Siegmann, William L.
Rensselaer Polytechnic Institute
Troy, NY 12181

Sinex, Dr. Charles
Building 8, Room 374
Applied Physics Laboratory
Johns Hopkins University
Johns Hopkins Rd.
Laurel, MD 20707

Spiesberger, Dr. John
Dept. of Ocean Engineering
Woods Hole Oceanographic Inst.
Woods Hole, MA 92543

Spindel, Dr. R. C.
Woods Hole Oceanographic Inst.
Dept. of Ocean Engineering
Woods Hole, MA 02543

Stanford, George
NORDA Code 115T
NSTL Station, MS 39529

Stickler, Dr. David
Courant Inst. of Mathematical
Sciences
New York University
251 Mercer Street
New York, NY 10012

Tappert, Prof. Fred
Rosentiel School of Marine and
Atmospheric Science
University of Miami
4600 Rickenbacker Causeway
Miami, FL 33149

Twersky, Dr. Victor
University of Illinois
Mathematics Department
Chicago, IL 60680

Vidmar, Dr. Paul J.
University of Texas
Applied Research Laboratories
P.O. Box 8029
Austin, TX 78712

Votaw, Dr. Charles
Naval Research Laboratory
Washington, DC 20360

Wales, Steve
Code 5120
Naval Research Laboratory
Washington, DC 20375

Wilson, Dr. James H.
Science Applications, International Corp.
9760 Owensmouth Avenue
Chatsworth, CA 91311

Ying-Yeung Yam
NAVSEA, 63D4
Washington, DC 20362

Young, CAPT E.
U.S. Naval Observatory
OP 952D
34th & Massachusetts Ave., N.W.
Washington, DC 20390

END

FILMED

7-85

DTIC